Vagus nerve stimulation promotes resolution of inflammation by a mechanism that involves Alox15 and requires the α7nAChR subunit

April S. Caravaca[a,b], Alessandro L. Gallina[a,b], Laura Tarnawski[a,b], Vladimir S. Shavva[a], Romain A. Colas[c], Jesmond Dalli[c], Stephen G. Malin[a], Henrik Hult[b,d], Hildur Arnardottir[a], and Peder S. Olofsson[a,b,e,1]

Nonresolving inflammation underlies a range of chronic inflammatory diseases, and therapeutic acceleration of resolution of inflammation may improve outcomes. Neural reflexes regulate the intensity of inflammation (for example, through signals in the vagus nerve), but whether activation of the vagus nerve promotes the resolution of inflammation in vivo has been unknown. To investigate this, mice were subjected to electrical vagus nerve stimulation (VNS) or sham surgery at the cervical level followed by zymosan-induced peritonitis. The duration of inflammation resolution was significantly reduced and efferocytosis was significantly increased in mice treated with VNS as compared with sham. Lipid mediator (LM) metabololipidomics revealed that mice treated with VNS had higher levels of specialized proresolving mediators (SPMs), particularly from the omega-3 docosahexaenoic (DHA) and docosapentaenoic (n-3 DPA) metabolomes, in peritoneal exudates. VNS also shifted the ratio between proinflammatory and proresolving LMs toward a proresolving profile, but this effect by VNS was inverted in mice deficient in 12/15-lipoxgenase (Alox15), a key enzyme in this SPM biosynthesis. The significant VNS-mediated reduction of neutrophil numbers in peritoneal exudates was absent in mice deficient in the cholinergic α7-nicotinic acetylcholine receptor subunit (α7nAChR), an essential component of the inflammatory reflex. Thus, VNS increased local levels of SPM and accelerated resolution of inflammation in zymosan-induced peritonitis by a mechanism that involves Alox15 and requires the α7nAChR.

vagus nerve | autonomic reflex | peritonitis | neuroinflammation | lipid mediators

Inflammation is essential for an effective antimicrobial defense and response to tissue injury, but it must be well regulated and ultimately resolved to avoid excessive tissue damage and development of inflammatory disease. An important mechanism to restore homeostasis is the active resolution of inflammation. Defective resolution may result in nonresolving inflammation, which underlies many chronic inflammatory diseases (1, 2). Key processes in the resolution of inflammation include the cessation of neutrophil infiltration and the promotion of macrophage reparative functions, including clearance of apoptotic cells from affected tissues by efferocytosis (3, 4). However, the mechanisms that regulate resolution of inflammation are not yet fully understood, and specific therapeutic options to actively promote inflammation resolution are lacking (5, 6).

It is becoming increasingly clear that the onset and intensity of inflammation are regulated by homeostatic neural reflexes, such as the "inflammatory reflex," in which the vagus nerve plays a key role (7, 8). Experimental studies over the past decades have demonstrated that vagus nerve stimulation (VNS) reduces the release of proinflammatory cytokines in acute inflammation (9–11). Rodents subjected to minutes-long VNS treatment show reduced proinflammatory cytokine release for ≥24 h (10–12); activation of this cholinergic anti-inflammatory pathway attenuates inflammation in experimental models of inflammatory diseases (7, 13–15), and VNS reduced levels of proinflammatory cytokines in clinical settings (16, 17). Consistent with these findings, 3 d after disruption of vagus nerve signaling by vagotomy, release of proinflammatory cytokines is increased in inflammation (18). Hence, animals subjected to prolonged disruption of vagus nerve signals by vagotomy respond more strongly to proinflammatory stimuli and show increased propensity for inflammation and higher inflammation-associated mortality (19, 20). This may potentially be explained by the loss of the homeostatic inhibition of inflammation that is normally conferred by the intact vagus nerve (7, 21). Interestingly, 1 wk after disruption of vagus nerve signaling by unilateral surgical vagotomy, peak numbers of neutrophils in zymosan-induced peritonitis are higher and the duration of neutrophil clearance is longer than in sham-treated mice (22). Consistent with these

Significance

Resolution of inflammation is an active process that restores tissue homeostasis and prevents the development of chronic inflammatory diseases. The mechanisms that regulate resolution of inflammation are only partially understood. Here, we showed that activation of the vagus nerve accelerated resolution of inflammation. Electrical stimulation of the vagus nerve in vivo increased levels of select specialized proresolving mediators in inflammation. Experiments in genetic mouse models revealed that the mechanism involved 12/15-lipoxgenase (Alox15), a key enzyme for biosynthesis of the identified mediators, and required the α7-nicotinic acetylcholine receptor subunit. The findings indicate that electrical signals in the vagus nerve activate a cholinergic signal promoting Alox15-dependent lipid mediator biosynthesis and accelerating resolution of inflammation, providing additional insights into neural regulation of inflammation.

[1]To whom correspondence may be addressed. Email: Peder.Olofsson@ki.se.

observations, levels of specialized proresolving mediators (SPMs), a class of potent bioactive lipid mediators (LMs) that actively regulate inflammation resolution, are significantly lower in vagotomized mice compared with sham (22). While it has been recently reported that stimulation of human and mouse vagus nerve ex vivo can enhance SPM production from the vagus nerve tissue itself (23), whether activation of the vagus nerve promotes resolution of inflammation and regulates proresolution mechanisms in inflammation in vivo remains to be determined. Here, we postulated that electrical VNS promotes resolution of inflammation in vivo.

Methods

Ethics Statement. This study and all experimental protocols were approved by the regional Stockholm Animal Research Ethics Committee (Stockholm, Sweden).

Animals. Male (age 10 to 16 wk) C57BL/6 (wild-type; Charles River Laboratories), $\alpha7$-nicotinic receptor–deficient (C57BL/6 background, B6.129S7-Chrna7tm1Bay/J, stock no. 003232 from The Jackson Laboratory), and 12/15-lipoxgenase (Alox15)–deficient (C57BL/6 background, B6.129S2-Alox15tm1Fun/J, stock no. 002778 from The Jackson Laboratory) mice were used. Mice were housed under a 12-h light/dark cycle with ad libitum access to food and water.

VNS. The surgery and method used for VNS have been previously described (12). In brief, following the induction of anesthesia with isoflurane, a ventral midline cervical incision was made, and subcutaneous tissues were retracted to expose the mandibular salivary glands. Proper exposure revealed the left neurovascular bundle containing the cervical vagus nerve, which was dissected away from the vasculature and isolated before being immobilized with a suture. The electrode was then placed under the nerve, and the suture was removed. Electrical stimulation of the left cervical vagus nerve was performed using stimulation set at current control, 1 mA, 250-μs biphasic pulse, 50-μs interphase delay, and 10 Hz for 5 min. Mice in the sham group were subjected to surgery but no nerve isolation or electrical stimulation.

Murine Peritonitis. After 1 h of recovery from VNS or sham surgery, 0.1 mg zymosan (Sigma-Aldrich) was administered intraperitoneally. Mice were killed by carbon dioxide asphyxiation at 4, 12, 24, and 48 h after zymosan challenge. Peritoneal exudates were collected by injecting 4 mL of phosphate-buffered saline (PBS) intraperitoneally, shaking the abdomen, and recovering ~3 mL of exudate. Cell counts were determined using an automated cell counter (Bio-Rad Laboratories), and the total numbers of cells of each population were determined by a BD FACSVerse flow cytometer (Becton Dickinson) normalized to the 4 mL of PBS that was initially injected.

Flow Cytometry Analysis. Cells were prepared for determining cellular composition by washing in PBS and fixating in 4% paraformaldehyde. Cells were incubated with anti-mouse CD16/CD32 mouse fragment crystallizable receptor block (Becton Dickinson) for 10 min and stained with anti-mouse F4/80 (clone: 1A8; eBioscience), anti-mouse CD11b (clone: M1/70.15; Invitrogen), and anti-mouse Ly6G (clone: 1A8; BioLegend) (*SI Appendix*, Fig. S1) for 30 min. For assessment of efferocytosis, cells were stained for extracellular anti-mouse F4/80, permeabilized for 10 min (eBioscience), and then stained for intracellular anti-mouse Ly6G (BioLegend) for 30 min (*SI Appendix*, Fig. S1). Cells were analyzed with a BD FACSVerse flow cytometer (Becton Dickinson).

Immunofluorescence. Mouse cells derived from peritoneal lavage (exudate) were collected after 12 h from zymosan intraperitoneal injection. Cells were then plated on fibronectin-coated (catalog no. F1141; Sigma-Aldrich) glass coverslips in Dulbecco's Modified Eagle Medium growth media (catalog no. 10565018; ThermoFisher) supplemented with 10% fetal bovine serum and 1% penicillin-streptomycin; after attachment for ~3 h, cells were fixed with 4% paraformaldehyde. Cells were then washed with 0.05% tris-buffered saline Triton (TBS-T). Blocking was performed with 3% bovine serum albumin and 3% normal horse serum in 0.05% TBS-T. Cells were then stained with a rat anti-mouse Ly-6G (clone 1A8; catalog no. 551459; BD Biosciences) and a rabbit polyclonal anti-mouse F4/80 (D4C8V; catalog no. 30325; Cell Signaling). Secondary antibodies were

conjugated with DyLight 488 and DyLight 594 (Vector Laboratories). Nuclei were stained with 4′,6-diamidino-2-phenylindole (DAPI), and slides were mounted with Dako mounting media (Agilent). Rabbit polyclonal immunoglobulin G (catalog no. ab171870; Abcam) was used as a negative control (*SI Appendix*, Fig. S2C). Images were acquired with a Nikon Eclipse T12 confocal microscope and processed with Fiji open-source software.

Liquid Chromatography–Tandem Mass Spectrometry–Based LM Metabololipidomics. Samples were extracted as described (24–26). In brief, 2 vol of ice-cold methanol containing deuterated internal standards (d$_8$-5S-HETE, d$_4$-LTB$_4$, d$_5$-LXA$_4$, d$_4$-PGE$_2$, d$_5$-RvD2, d$_5$-MaR1, d$_5$-MaR2, d$_5$-RvD3, d$_5$-RvE1, and d$_5$-17R-RvD1) representing each chromatographic region of an identified LM was added to inflammatory peritoneal exudates. Following protein precipitation ($-20\,°C$ for a minimum of 45 min), supernatants were extracted on an ExtraHera instrument (Biotage) using solid-phase extraction with Isolute C18 500-mg columns (Biotage). Methyl formate fractions were collected, brought to dryness, and resuspended in phase (methanol/water, 1:1 [vol/vol]) for injection on a Shimadzu LC-20AD HPLC and a Shimadzu SIL-20AC autoinjector paired with a QTrap 6500+ (Sciex). An Agilent Poroshell 120 EC-C18 column (100 mm × 4.6 mm × 2.7 μm) was kept at 50 °C, and mediators were eluted using a mobile phase consisting of methanol/water/acetic acid of 20:80:0.01 (vol/vol/vol) that was ramped to 50:50:0.01 (vol/vol/vol) over 0.5 min and then, to 80:20:0.01 (vol/vol/vol) from 2 to 11 min, maintained until 14.5 min, and then, rapidly ramped to 98:2:0.01 (vol/vol/vol) for the next 0.1 min. This was subsequently maintained at 98:2:0.01 (vol/vol/vol) for 5.4 min, and the flow rate was maintained at 0.5 mL/min. QTrap 6500+ was operated in negative mode using a multiple reaction monitoring method. Each LM was identified and quantified using the following criteria: 1) presence of a peak at a retention time corresponding with the relevant standard, 2) eight or more data points, and 3) a signal to noise ratio greater than five (25, 27). Calibration curves were obtained for each using synthetic compound mixtures at 0.78, 1.56, 3.12, 6.25, 12.5, 25, 50, 100, and 200 pg that gave linear calibration curves with r^2 values of 0.98 to 0.99.

Resolution Indices and Inflammation Decay. Resolution indices were calculated with the previously described method (28) and with an exponential decay model. The resolution indices are defined as the time (T_{max}) of maximum neutrophil count (Ψ_{max}) and the time point (T_{50}) when the neutrophil count reaches 50% (Ψ_{50}) of Ψ_{max}. The resolution interval (R_i) is the time interval that it takes for neutrophils to decrease from Ψ_{max} to Ψ_{50} ($R_i = T_{max} - T_{50}$) (28).

In the exponential decay model, the neutrophil count is assumed to decay exponentially at a rate $\beta > 0$ after some unobserved time t_0. More precisely, the neutrophil count $x(t)$ at time t is assumed to be given by $x(t) = x(t_0)e^{-\beta(t-t_0)}$ for $t > t_0$. By taking logarithms, it follows that $-\ln(x(t)) = \alpha + \beta t$, where $\alpha = -\ln(x(t_0)) - \beta t_0$. Consequently, by taking minus the logarithm of the measurements at times $t_i > t_0$, we may use a linear regression model of the form $-\ln(y(t_i)) = \alpha + \beta t_i + \varepsilon_i$ to estimate and test hypotheses about the exponential decay rate β. Moreover, by assuming that the exponential decay rate model is valid after the peak measurement, the resolution time can be expressed as $T_{1/2} = \ln(2)/\beta$.

For visualization of the course of inflammation as represented by neutrophil counts over time, an ordinary differential equation (ODE) model was used. The observed neutrophil counts at the measurement times may be modeled as noisy observations of the population mean, where the population mean, x_1, is the first component of the solution to a system of ODEs $\dot{x}(t) = f(x(t))$. For instance, with one latent auxiliary process, $x_2(t)$, a potential model is given by $\dot{x}_1(t) = [\alpha\, g_K(x_2(t)) - \gamma]x_1(t)$, $\dot{x}_2(t) = -\beta\, g_K(x_2(t))$, with $g_K(x) = x/(x+K)$. In this model, the latent variable $x_2(t)$ may be interpreted as a substrate that increases the neutrophil count in the early stage of inflammation, $\dot{x}_1(t) > 0$. As the substrate is consumed, the inflammation resolves, and the neutrophil count decreases, $\dot{x}_1(t) < 0$.

Treatment of Mice with Specialized Proresolving Mediators. Resolvin D2 (RvD2), RvD5, 17R-RvD3, and maresin R2 (MaR2) were obtained from Cayman Chemical Company. Mice were injected intraperitoneally with a mixture of SPM containing 50 ng of each compound in PBS (200 μL/mouse) or vehicle (1.25% EtOH [vol/vol]) control in PBS (200 μL/mouse).

Cytokine Analysis. Supernatants from peritoneal exudates were analyzed using the U-Plex Biomarker Group 1 (mouse) kit (Meso Scale Discovery), and concentrations of interleukin (IL)-10, IL-1β, IL-6, keratinocytes-derived chemokine (KC; CXCL1), and tumor necrosis factor (TNF) were determined.

Statistics. Values are shown as mean ± SEM unless otherwise stated. Differences between groups were analyzed using unpaired, one-tailed, or two-tailed Student's t tests or two-way ANOVA followed by Fisher's least significant difference post hoc test as appropriate. Grubbs' outlier test was used as applicable. $P \leq 0.05$ was considered significant. These statistical calculations were performed using the Prism 8 software (GraphPad software). R package ggplot2 was used for visualization of ODE and linear models (H. Wickham, ggplot2: Elegant Graphics for Data Analysis). For analysis of mass spectrometry data, partial least squares discrimination analysis (PLS-DA) was performed using MetaboAnalyst v5.0 (https://www.metaboanalyst.ca/MetaboAnalyst/ModuleView.xhtml) following mean centering and unit variance scaling of LM levels. After normalizing concentrations (expressed as fold change from sham-treated mice), LM profiles were subjected to interaction network pathway analysis using Cytoscape (https://cytoscape.org/).

Results

Electrical VNS Shortened the Resolution Time and Increased Efferocytosis in Zymosan-Induced Peritonitis.

Wild-type mice were subjected to left cervical VNS or sham treatment followed by peritonitis induced using intraperitoneal injection of yeast cell wall particles (zymosan). The zymosan dose was titrated to induce a strong inflammatory response within a biologically relevant range (*SI Appendix*, Fig. S2A). Peritoneal exudates were collected at consecutive time points, and the neutrophil numbers were quantified using flow cytometry (*SI Appendix*, Fig. S1). The dynamic changes in peritoneal neutrophil numbers were plotted as a function of time to visualize the course of inflammation, and resolution indices were then determined (*SI Appendix*, Fig. S2B) as previously described (28–30) and are detailed in *Methods*. Calculation of the resolution interval (R_i) (25) showed an average R_i of 12.5 h in sham-treated mice and 8 h in VNS-treated mice, which correspond to a 36% reduction in R_i following VNS treatment compared with sham (*SI Appendix*, Fig. S2B).

Since neutrophil count measurements are taken hours apart, the peak neutrophil value may often not be observed, which precludes precise calculation of the true resolution time as previously defined (28). Large variations in peak neutrophil infiltration numbers between experimental conditions may further complicate the interpretation of the resolution time (28–30). To address this and enable mathematical analysis of the inflammation kinetics, we used an ODE model. The observed neutrophil counts at the measurement times were modeled as noisy observations of the population mean, where the population mean, x_1, is the first component of the solution to a system of ODEs $\dot{x}(t) = f(x(t))$, which were plotted (Fig. 1A). Calculation of the R_i using the model showed an R_i of 15.6 h in sham-treated mice and 10.3 h in VNS-treated mice, corresponding to a 34% reduction in R_i following VNS treatment compared with sham (Fig. 1A), which agrees closely with the established method (*SI Appendix*, Fig. S2B). We observed that the inflammation decay, reflected by reduced neutrophil counts, was exponential as evidenced by analysis of several published datasets of zymosan-induced peritonitis in wild-type mice (*SI Appendix*, Fig. S3) (30, 31). Accordingly, we used an exponential decay model to calculate the resolution rate. The slope represents the inflammation decay (I_d) (Fig. 1B). Of note, this approach obviates the need to determine the time and value of the peak neutrophil levels and permits direct comparison of the rates of inflammation resolution between different experimental groups and of the resolution time $T_{1/2} =$ $\ln(2)/I_d$, where I_d is the decay rate of neutrophil numbers. The approach also enables focus on the rate with which inflammation decays, irrespective of the intensity of inflammation, thus providing a useful measurement specifically of the speed of resolution. We observed that the rate of inflammation resolution (I_d) was significantly higher in the VNS-treated group compared with sham (Fig. 1C).

The observed difference in mean neutrophil counts between VNS- and sham-treated animals was largest at the 12-h time point (Fig. 1D), as were observed differences in cytokine levels (Fig. 1E and *SI Appendix*, Fig. S4). The 12-h time point was accordingly selected for further examination. In supernatants of peritoneal exudates collected 12 h after zymosan challenge, IL-6 and IL-1β levels were significantly lower in VNS-treated mice compared with sham, while levels of TNF, IL-10, and the neutrophil chemoattractant CXCL1 were not significantly different between groups (Fig. 1E). Clearance of apoptotic neutrophils (efferocytosis) and cellular debris is a key component of the inflammation resolution process. Hence, we next investigated the effect of VNS on macrophage efferocytosis and observed macrophage clearance of neutrophils in the peritoneal exudates at 12 h as evidenced by the presence of F4/80⁺ cells (macrophages) containing intracellular Ly6G⁺ cells (neutrophils) by immunofluorescent analysis (Fig. 1F and *SI Appendix*, Fig. S2C). Flow cytometry showed a significantly higher number of F4/80⁺Ly6G⁺ cells in exudates from VNS-treated mice as compared with sham (Fig. 1G and *SI Appendix*, Fig. S1 E and F), indicating increased efferocytosis in vivo in the VNS-treated group. Thus, VNS treatment regulates neutrophil numbers, efferocytosis, and the rate of inflammation resolution in zymosan-induced peritonitis.

VNS Enhanced Endogenous SPM Production In Vivo.

Since resolution of inflammation is regulated by SPMs, which are known to promote macrophage efferocytosis and counterregulate proinflammatory cytokines (1, 32), we investigated whether VNS regulates SPM production in acute peritonitis. Peritoneal LM levels in exudates from mice subjected to zymosan-induced peritonitis were determined using liquid chromatography–tandem mass spectrometry (LC-MS/MS)–based LM metabololipidomics (33). We identified mediators from all four major bioactive metabolomes (Table 1), which include the Resolvins (Rv) (E, D and T series), protectins (PD), and maresins (MaR) from the omega-3 docosahexaenoic (DHA); docosapentaenoic (n-3 DPA) and eicosapentanoic (EPA) metabolomes; and the arachidonic acid (AA)–derived lipoxins (LXA), leukotrienes (LT), thromboxanes (TX), and prostaglandins (PG) from the omega-6 metabolome (Table 1). To evaluate whether LM profiles were different between VNS- and sham-treated mice, we performed PLS-DA, a regression model that identifies variables (i.e., LMs) contributing to the separation of experimental groups (34). In this analysis, we observed that samples from VNS and sham groups were segregated (Fig. 2 A, Left). Analysis of individual mediators in terms of their variable importance in projection (VIP) score, which provides a measure of the contribution of each mediator in the observed separation between the two groups (35), revealed that several DHA- and n-3 DPA–derived LMs contributed to the segregation and were positively associated with the VNS group, including the DHA-derived MaR2, RvD2, RvD5, and 17R-RvD3 as well as the n-3 DPA–derived 10S,17S-diHDPA and PD2ₙ₋₃ ᴅᴘᴀ (Fig. 2 A, Right and Table 1). Concentrations of total DHA-derived RvD, PD, and MaR as well as n-3 DPA–derived PD were all significantly higher in the VNS-treated group when compared with sham (Fig. 2 B and C and Table 1). There was no significant difference
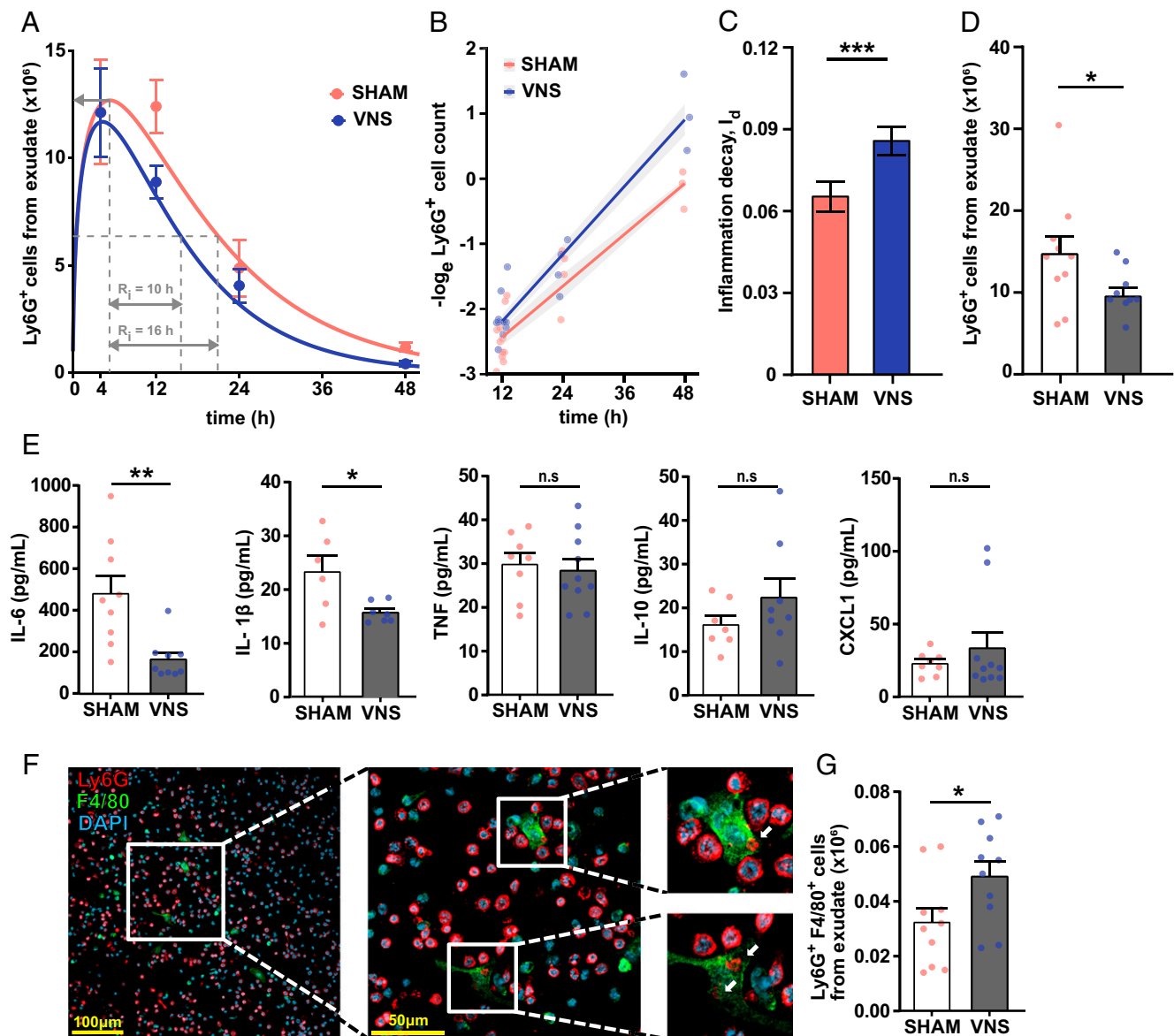
Fig. 1. Electrical VNS promoted resolution of inflammation in zymosan-induced peritonitis. Wild-type mice were subjected to either left cervical VNS (blue dots or blue/gray bars) or sham surgery (red dots or red/open bars) followed by intraperitoneal injection of zymosan (0.1 mg/mouse) after 1 h. Peritoneal exudates were collected at indicated time points after zymosan challenge and analyzed by flow cytometry. (A) The numbers of Ly6G$^+$ cells were plotted over time (dots) and modeled using an ODE model (lines). Classic resolution indices were also determined (dashed gray lines): Ψ_{max} (maximal neutrophil infiltration), and R_i (resolution interval; the time interval from Ψ_{max} to Ψ_{50}). (B) The log$_e$ cell counts (dots) plotted over time and linear regression analysis (lines), with shaded areas indicating the mean squared error. (C) Rate of inflammation resolution expressed as the inflammation decay (I_d) in sham (red) and VNS-treated (blue) mice. Results in A–C are from n = 2 to 5 experiments. (D) Peritoneal exudate Ly6G$^+$ cell counts in sham (red) and VNS-treated (blue) mice at 12 h after zymosan-induced peritonitis. n = 5 experiments. (E) Cytokine/chemokine concentrations were measured in supernatants of peritoneal exudates collected from VNS- (blue) and sham-treated (red) mice at 12 h after intraperitoneal zymosan injection using the Meso Scale Discovery multiplex assay. n = 3 experiments. (F) Peritoneal exudate was collected at 12 h after zymosan-induced peritonitis. Cells were plated in vitro and stained using anti-Ly6G (red) and anti-F4/80 (green) antibodies. DAPI (blue) was used to visualize cell nuclei. Cells were imaged using a Nikon confocal microscope. White arrows indicate Ly6G$^+$ regions within F4/80$^+$ cells. (G) Efferocytosis plotted as absolute numbers of F480$^+$Ly6G$^+$ cells measured by flow cytometry following fixation and intracellular Ly6G staining of peritoneal exudate collected at 12 h after zymosan-induced peritonitis. Results are expressed as mean ± SEM. n.s = not significant; *$P < 0.05$; **$P < 0.01$; ***$P < 0.001$.

between VNS- and sham-treated groups in EPA- or AA-derived SPM nor in the cyclooxygenase-derived and lipoxygenase-derived proinflammatory LMs (Fig. 2B). In line with this, there was a significantly lower proinflammatory prostanoid to SPM ratio in the VNS-treated group (Fig. 2D), shifting the balance of the observed LMs toward a more proresolving state.

Next, differences between VNS- and sham-treated groups of individual LMs were plotted after LM interaction network pathway analysis (Fig. 2E) to estimate activity in individual metabolic pathways. The analysis identified higher relative levels of Alox15-derived mediators from the DHA and n-3 DPA metabolomes, including the DHA-derived RvD2 and RvD5,

and the n-3 DPA–derived PD2$_{n-3}$ $_{DPA}$ in the VNS-treated group compared with sham (Fig. 2E and Table 1). Together, these observations indicate that VNS treatment shifted the local exudate LM content in peritonitis toward a more proresolving state and suggest that signals in the vagus nerve regulate Alox15 activity.

Alox15 Was Involved in Vagus Nerve–Mediated Regulation of Resolution of Inflammation. To investigate whether LMs in the Alox15 pathway mediate VNS-dependent regulation of inflammation resolution, we used a genetic strategy. Alox15-deficient mice were subjected to VNS or sham surgery followed

Table 1. LM profiles in peritoneal exudates of wild-type, Alox15-deficient, and α7nAChR-deficient mice subjected to VNS or sham treatment prior to zymosan-induced peritonitis

Mediator	C57BL/6		Alox15-deficient		α7nAChR-deficient	
	Sham	VNS	Sham	VNS	Sham	VNS
RvD1	0.1 ± 0.3	0.4 ± 0.6	1.3 ± 0.3	0.5 ± 0.3	0.7 ± 0.3	6.3 ± 4.3
RvD2	1.1 ± 0.8	5.5 ± 3.2**	73.1 ± 40.7	0.9 ± 0.7	2.0 ± 0.6	13.1 ± 7.8
RvD3	0.0 ± 0.0	0.0 ± 0.0	0.1 ± 0.1	0.0 ± 0.0	0.0 ± 0.0	0.7 ± 0.4
RvD4	2.6 ± 2.3	2.2 ± 1.4	2.4 ± 0.7	0.8 ± 0.5	1.1 ± 0.3	14.7 ± 9.4
RvD5	2.0 ± 1.2	4.4 ± 2.5	1.2 ± 0.4	0.7 ± 0.3	2.3 ± 0.7	8.8 ± 2.6*
RvD6	0.7 ± 0.8	0.8 ± 1.4	2.5 ± 0.4	0.9 ± 0.6	2.3 ± 1.3	14.8 ± 6.2
17R-RvD1	0.0 ± 0.0	0.0 ± 0.0	0.1 ± 0.1	0.0 ± 0.0	0.1 ± 0.1	0.4 ± 0.2
17R-RvD3	0.3 ± 0.2	1.0 ± 0.9	0.0 ± 0.0	0.0 ± 0.0	0.0 ± 0.0	0.2 ± 0.2
PD1	0.0 ± 0.0	0.0 ± 0.0	0.7 ± 0.3	0.4 ± 0.2	0.5 ± 0.2	7.8 ± 5.3
17R-PD1	0.8 ± 0.4	1.8 ± 0.9*	0.5 ± 0.3	0.2 ± 0.2	0.3 ± 0.2	0.8 ± 0.3
10S.17S-diHDHA	26.3 ± 14.6	85.4 ± 48.8*	2.3 ± 0.5	0.6 ± 0.5	8.5 ± 1.9	39.0 ± 13.9
22-OH-PD1	0.0 ± 0.0	0.0 ± 0.0	0.0 ± 0.0	0.0 ± 0.0	0.0 ± 0.0	0.0 ± 0.0
MaR1	0.0 ± 0.0	0.0 ± 0.0	0.3 ± 0.2	0.1 ± 0.1	3.0 ± 0.8	9.2 ± 2.6
MaR2	3.1 ± 2.5	17.0 ± 10.5*	0.7 ± 0.4	0.0 ± 0.0	3.3 ± 0.8	14.2 ± 3.6*
7S.14S-diHDHA	3.2 ± 1.8	13.3 ± 10.3*	1.9 ± 0.5	0.2 ± 0.1*	3.8 ± 1.3	24.7 ± 9.0*
4.14-diHDHA	2.9 ± 1.3	9.0 ± 6.1*	8.8 ± 1.3	3.1 ± 2.4	10.1 ± 5.0	51.5 ± 21.1
RvT1	0.3 ± 0.3	0.9 ± 0.5	1.1 ± 0.2	0.4 ± 0.2	1.1 ± 0.4	4.8 ± 2.5
RvT2	0.0 ± 0.0	0.0 ± 0.0	0.0 ± 0.0	0.1 ± 0.1	0.0 ± 0.0	0.2 ± 0.2
RvT3	0.0 ± 0.0	0.0 ± 0.0	0.0 ± 0.0	0.0 ± 0.0	0.0 ± 0.0	0.0 ± 0.0
RvT4	0.5 ± 0.4	0.5 ± 0.5	1.0 ± 0.4	0.8 ± 0.8	1.0 ± 0.5	12.3 ± 6.9
RvD1$_{n-3 DPA}$	0.1 ± 0.1	0.1 ± 0.2	1.2 ± 0.2	0.2 ± 0.2*	0.9 ± 0.4	5.1 ± 1.8
RvD2$_{n-3 DPA}$	0.0 ± 0.0	0.0 ± 0.0	1.5 ± 1.5	0.0 ± 0.0	0.2 ± 0.1	0.3 ± 0.1
RvD5$_{n-3 DPA}$	0.1 ± 0.3	0.6 ± 0.6	1.3 ± 0.3	0.2 ± 0.2*	0.7 ± 0.4	8.1 ± 4.0
PD1$_{n-3 DPA}$	0.0 ± 0.0	0.0 ± 0.0	0.0 ± 0.0	0.0 ± 0.0	0.0 ± 0.0	0.0 ± 0.0
PD2$_{n-3 DPA}$	1.7 ± 1.0	4.6 ± 3.2	0.0 ± 0.0	0.0 ± 0.0	0.4 ± 0.2	2.5 ± 1.2
10S. 17S-diHDPA	0.1 ± 0.1	1.1 ± 0.7**	0.0 ± 0.0	0.0 ± 0.0	0.1 ± 0.1	0.9 ± 0.5*
MaR1$_{n-3 DPA}$	0.0 ± 0.0	0.0 ± 0.0	0.0 ± 0.0	0.0 ± 0.0	0.0 ± 0.0	0.0 ± 0.0
MaR2$_{n-3 DPA}$	3.9 ± 0.8	4.0 ± 1.3	9.3 ± 0.7	10.5 ± 1.1	7.5 ± 0.7	11.7 ± 2.2
7S.14S-diHDPA	0.0 ± 0.0	0.0 ± 0.0	0.7 ± 0.1	0.3 ± 0.2	1.6 ± 0.2	8.5 ± 2.5
RvE1	0.0 ± 0.1	0.2 ± 0.4	0.0 ± 0.0	0.0 ± 0.0	0.0 ± 0.0	0.7 ± 0.2
RvE2	1.4 ± 3.1	0.2 ± 0.5	0.3 ± 0.2	0.2 ± 0.2	0.8 ± 0.5	5.9 ± 2.5
RvE3	0.0 ± 0.0	0.0 ± 0.0	1.3 ± 0.2	0.6 ± 0.2	1.9 ± 1.1	8.4 ± 4.6
LXA$_4$	0.0 ± 0.0	0.0 ± 0.0	19.5 ± 16.8	7.8 ± 7.4	8.2 ± 3.7	128.9 ± 76.2
LXB$_4$	0.0 ± 0.0	0.0 ± 0.0	167.1 ± 39.7	32.7 ± 23.2*	51.7 ± 19.2	253.8 ± 134.3
5S.15S-diHETE	16.0 ± 10.9	14.3 ± 11.9	29.6 ± 5.0	5.8 ± 2.9**	28.0 ± 15.3	163.5 ± 62.2
15-epi-LXA$_4$	47.4 ± 33.6	62.6 ± 88.6	130.4 ± 30.7	29.8 ± 15.3*	78.9 ± 19.4	681.2 ± 424.1
15-epi-LXB$_4$	0.0 ± 0.0	0.0 ± 0.0	0.0 ± 0.0	0.0 ± 0.0	1.8 ± 1.6	3.7 ± 2.4
LTB$_4$	21.8 ± 4.0	68.9 ± 60.5	7.3 ± 0.8	4.6 ± 2.1	9.3 ± 3.6	51.5 ± 33.5
5S.12S-diHETE	37.2 ± 14.3	89.6 ± 75.8	25.7 ± 6.3	6.6 ± 4.3*	24.7 ± 9.7	161.1 ± 52.3*
6-trans-LTB$_4$	36.3 ± 10.0	89.1 ± 60.9	7.9 ± 0.7	2.9 ± 1.0**	15.3 ± 4.2	60.6 ± 8.3**
6-trans-12-epi LTB$_4$	26.0 ± 11.1	75.2 ± 50.4*	8.4 ± 1.2	2.9 ± 1.2*	14.4 ± 2.9	54.9 ± 9.6**
20-OH-LTB$_4$	0.3 ± 0.2	0.3 ± 0.3	0.1 ± 0.0	0.1 ± 0.0	0.1 ± 0.0	0.5 ± 0.2*
PGD$_2$	155.6 ± 138.7	146.5 ± 66.7	9.2 ± 1.3	9.8 ± 1.6	4.2 ± 0.6	19.8 ± 10.4
PGE$_2$	354.6 ± 166.2	305.3 ± 90.8	41.3 ± 13.2	19.7 ± 4.2	23.3 ± 4.2	179.9 ± 122.4
PGF$_{2\alpha}$	67.4 ± 28.2	51.9 ± 14.8	17.3 ± 8.5	11.4 ± 1.9	8.4 ± 1.3	24.0 ± 6.7*
TxB$_2$	121.2 ± 83.4	141.2 ± 38.5	11.0 ± 1.9	7.6 ± 0.7	5.6 ± 1.0	24.4 ± 9.7*

Wild-type and Alox15- and α7nAChR-deficient mice were subjected to VNS or sham surgery and injected with zymosan (0.1 mg/mouse) intraperitoneally. Peritoneal exudates were collected 12 h after zymosan challenge. LM levels were measured using LC-MS/MS. Results are shown as mean ± SEM of picograms per exudate. *$P < 0.05$; **$P < 0.01$. Rv - Resolvin, MaR - Maresin, PD - Protectin, LX - Lipoxin, LT - Leukotriene, PG - Prostaglandin, Tx - Thromboxane, HETE - Hydroxyeicosatetraenoic acid.

by zymosan injection. Peritoneal exudates were collected, and neutrophil numbers were quantified and plotted (Fig. 3*A*). The exponential decay model was used to calculate the inflammation decay (I_d, i.e., the rate of inflammation resolution) (Fig. 3*B*). There was no significant difference in I_d between VNS- and sham-treated Alox15-deficient mice (Fig. 3*C*). Numbers of Ly6G$^+$ neutrophils (Fig. 3*D*) and efferocytosis as reflected by the numbers of Ly6G$^+$F4/80$^+$ cells (Fig. 3*E* and *SI Appendix,* Fig. S5*C*) in peritoneal exudates were not significantly different between VNS- and sham-treated mice 12 or 24 h after

intraperitoneal injection of zymosan. Furthermore, levels of IL-1β, IL-6, IL-10, TNF, and CXCL1 in peritoneal exudates collected 12 and 24 h after zymosan injection were not significantly different between VNS- and sham-treated Alox15-deficient mice (*SI Appendix,* Fig. S5 *A and B*). LC-MS/MS (33) analysis of peritoneal exudates showed a skewed LM profile in Alox15-deficient mice with, as expected, a relative absence of the Alox15-dependent PDs (PD and PD$_{n-3 DPA}$) (Fig. 3*F*), corroborating the loss of the Alox15 enzyme. There was significant segregation between the LM profiles in peritoneal exudates from
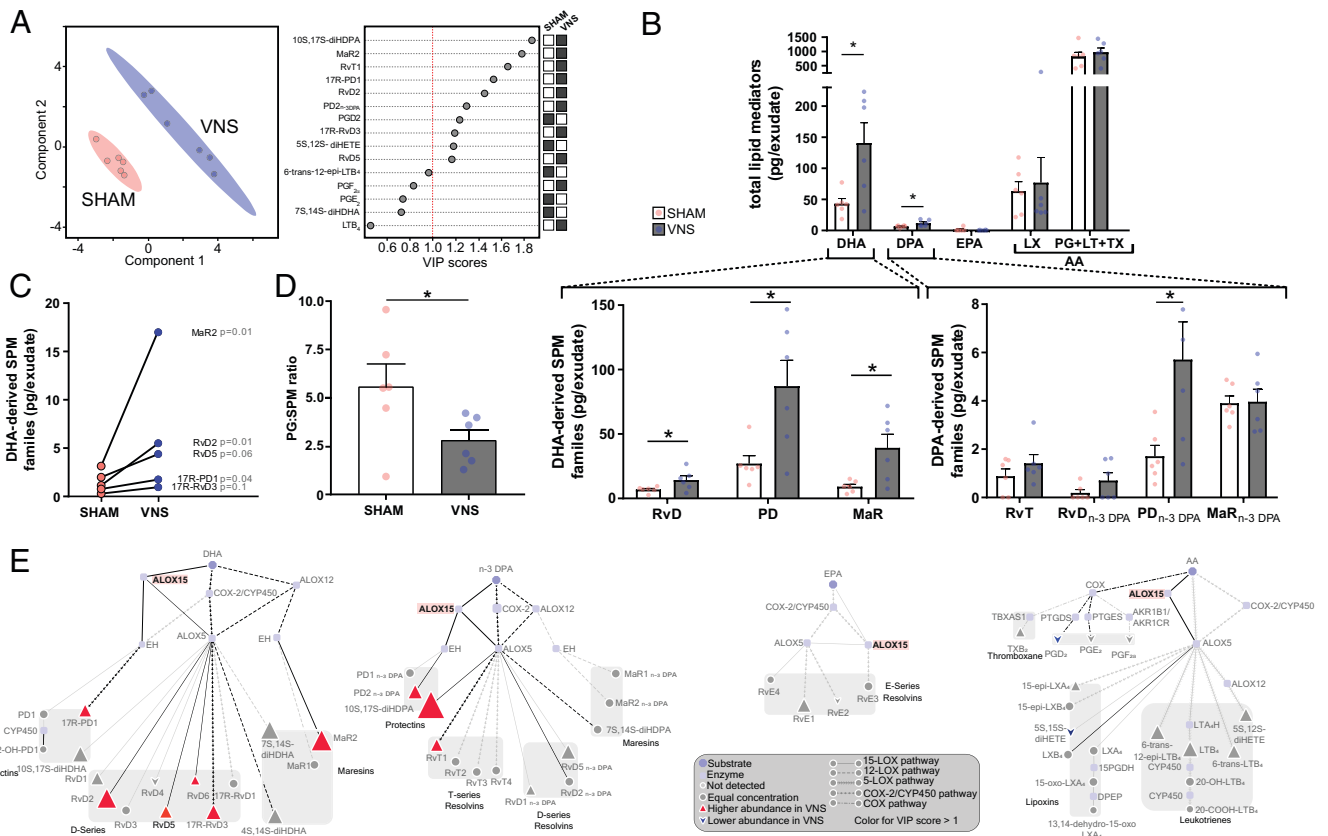
Fig. 2. VNS increased levels of lipoxygenase-derived SPM. Wild-type mice were subjected to either left cervical VNS or sham surgery followed by peritoneal injection of zymosan (0.1 mg/mouse). Levels of LMs in peritoneal exudates collected 12 h after intraperitoneal zymosan injection were measured using LC-MS/MS–based LM profiling. Concentrations of identified and quantified LMs were analyzed using PLS-DA, generating (*A*) a two-dimensional score plot showing a separation between VNS (blue) and sham-treated (red) groups (*Left*) and VIP scores of 15 LMs with the greatest contribution to the separation of the groups (*Right*). White squares indicate lower levels and black squares indicate higher levels in the sham or VNS-treated group. (*B*) Levels of total LMs identified in peritoneal exudate collected at 12 h after zymosan-induced peritonitis from the major bioactive metabolomes DHA, EPA, n-3 DPA, and AA (LX and PG + LT + TX). Levels of identified DHA-derived (*Lower Left*) and n-3 DPA–derived (*Lower Right*) SPM families in peritoneal exudates and VNS- (blue dots and gray bars) and sham-treated (red dots and open bars) mice are shown. (*C*) Levels of select DHA-derived SPM in sham- or VNS-treated mice. (*D*) Ratio of proinflammatory PGs to SPM in peritoneal exudates from VNS (blue dots and gray bar) and sham-treated (red dots and open bar) mice. (*E*) LM profiles in VNS- and sham-treated mice were investigated using an interaction network pathway analysis. $n = 2$ experiments. Data in *B* and *D* are shown as mean ± SEM. *$P < 0.05$.

zymosan-injected VNS- and sham-treated Alox15-deficient mice as evidenced by PLS-DA (Fig. 3*G* and *SI Appendix*, Fig. S5*D*). Surprisingly, the segregation was explained by lower mean levels of the measured LMs in VNS-treated compared with sham-treated Alox15-deficient mice (Fig. 3*F*), as also reflected in the LM interaction network pathway analysis (Fig. 3*I*). The PG/SPM ratio was increased by VNS in Alox15-deficient mice (Fig. 3*H*), and the ratio thus inverted compared with our findings in VNS-treated wild-type mice (Fig. 2*D*).

Vagus Nerve–Mediated Regulation of Inflammation Resolution Required the α7 Nicotinic Acetylcholine Receptor Subunit. In zymosan-induced peritonitis in wild-type mice, VNS strongly up-regulated PD and PD$_{n-3\ DPA}$, which share a biosynthetic pathway through Alox15 with the protectin conjugate in tissue regeneration (PCTR) family (Fig. 2*B*). In lymphoid cells, the PD and PCTR pathway marker, the Alox15-derived 17-hydroxy-DHA, is up-regulated by acetylcholine (ACh) (29), the primary neurotransmitter of the vagus nerve. Peritoneal ACh is decreased after disruption of the vagus nerve and associated with alterations in the peritoneal LM profile (29), but the target receptor for ACh in this context is unknown. The α7-nicotinic acetylcholine receptor subunit (α7nAChR) is expressed on immune cells and is an essential regulator of inflammation (13,15). To investigate whether the

α7nAChR is a target receptor for VNS-mediated regulation of resolution of inflammation, we subjected mice deficient in the α7nAChR to VNS or sham surgery followed by zymosan-induced peritonitis. There was no significant difference in the course of inflammation as measured by neutrophil numbers in the peritoneal cavity over time (Fig. 4*A*). There was also no significant difference in the inflammation decay rate (I_d) between VNS- or sham-treated groups (Fig. 4 *B* and *C*). Mean numbers of neutrophils in peritoneal exudates were similar (Fig. 4*D*), and there was no significant difference in efferocytosis (Fig. 4*E*) or levels of cytokines/chemokines (*SI Appendix*, Fig. S6 *A* and *B*) between VNS- and sham-treated groups, supporting an essential role for α7nAChR in VNS-mediated regulation of resolution of zymosan-induced peritonitis.

Analysis of the peritoneal exudates from VNS- and sham-treated α7nAChR-deficient mice using LC-MS/MS revealed a marked increase in all LMs measured, with only the MaR$_{n-3\ DPA}$ reaching statistical significance, in the VNS-treated group (Fig. 4*F*). Of note, there was no significant difference in the PG/SPM ratio between VNS- and sham-treated α7nAChR mice (Fig. 4*G*), implying that the LM balance did not change toward a more proresolving nor proinflammatory profile. While there was segregation in terms of the totality of analyzed LMs between the experimental groups as demonstrated by PLS-DA, the separation was less pronounced than in wild-type and
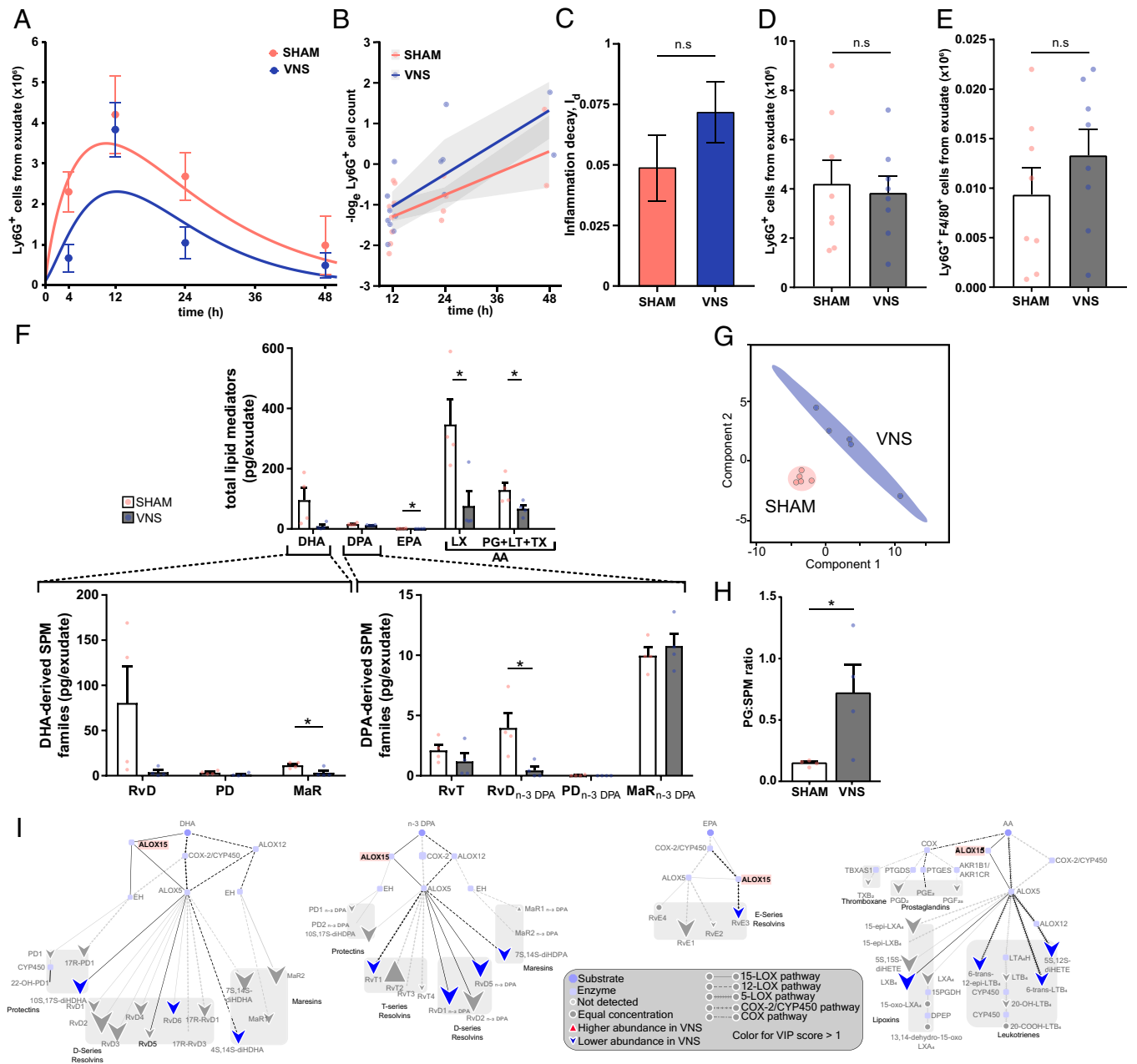
Fig. 3. Alox15 was involved in vagus nerve–mediated regulation of resolution of inflammation. Alox15-deficient mice were subjected to either left cervical VNS or sham surgery followed by peritoneal injection of zymosan. Peritoneal exudates were collected at indicated time points after zymosan challenge and analyzed by flow cytometry. (*A*) Ly6G$^+$ cells were plotted over time using an ODE model. (*B*) The log$_e$ cell counts (dots) plotted over time and linear regression analysis (lines), with shaded areas indicating the mean squared error. (*C*) Rate of inflammation resolution expressed as the inflammation decay (I_d) in sham- (red) and VNS-treated (blue) mice. Results in *A*–*C* are from *n* = 2 experiments. (*D*) Peritoneal exudate Ly6G$^+$ cell counts in sham- (red) and VNS-treated (blue) mice at 12 h after zymosan-induced peritonitis. (*E*) Efferocytosis plotted as absolute numbers of F4/80$^+$Ly6G$^+$ cells measured by flow cytometry following fixation and intracellular Ly6G staining of peritoneal exudate collected at 12 h after zymosan-induced peritonitis. Results in *D* and *E* are from *n* = 3 experiments. (*F*) Levels of total LMs identified in peritoneal exudate collected at 12 h after zymosan-induced peritonitis from the major bioactive metabolome families DHA, DPA, EPA, and AA (LX and PG + LT + TX). Levels of identified DHA-derived SPM families (*Lower Left*) and n-3 DPA–derived SPM families (*Lower Right*) in peritoneal exudates from VNS- (blue dots and gray bars) and sham-treated (red dots and open bars) Alox15-deficient mice. Concentrations of identified and quantified LMs were analyzed using PLS-DA, generating (*G*) a two-dimensional score plot of LMs identified in peritoneal exudates from VNS- (blue) and sham-treated (red) mice. (*H*) Ratios of proinflammatory PGs to SPM in peritoneal exudates from VNS- (blue dots and gray bar) and sham-treated (red dots and open bar) Alox15-deficient mice. (*I*) LM profiles in VNS- and sham-treated Alox15-deficient mice were investigated using an interaction network pathway analysis. Results in *F*–*I* are from *n* = 2 experiments. Results in *C*–*F* are shown as mean ± SEM. n.s = not significant; *P < 0.05.

Alox15-deficient mice (Fig. 4*H* and *SI Appendix*, Fig. S6*C*). LM interaction network pathway analysis showed that members of the PDs, MaRs, D-series Rvs, TX, PGs, and LTs all contributed to the segregation of VNS- and sham-treated samples (Fig. 4*I*). Together, these observations show that while VNS in α7nAChR-deficient mice up-regulated the levels of all exudate LMs independent of the enzymatic pathway, it did not significantly change the PG/SPM balance or the inflammation decay

rate. Hence, α7nAChR was essential for VNS-mediated regulation of the inflammation decay rate.

To study mechanism further, α7nAChR-deficient mice were injected intraperitoneally with vehicle or a mixture of SPM containing commercially available key SPM induced by VNS in wild-type mouse peritonitis (Fig. 2*C* and Table 1) (i.e., MaR2, RvD2, RvD5, and 17R-RvD3) and subjected to zymosan-induced peritonitis. At 12 h after induction of
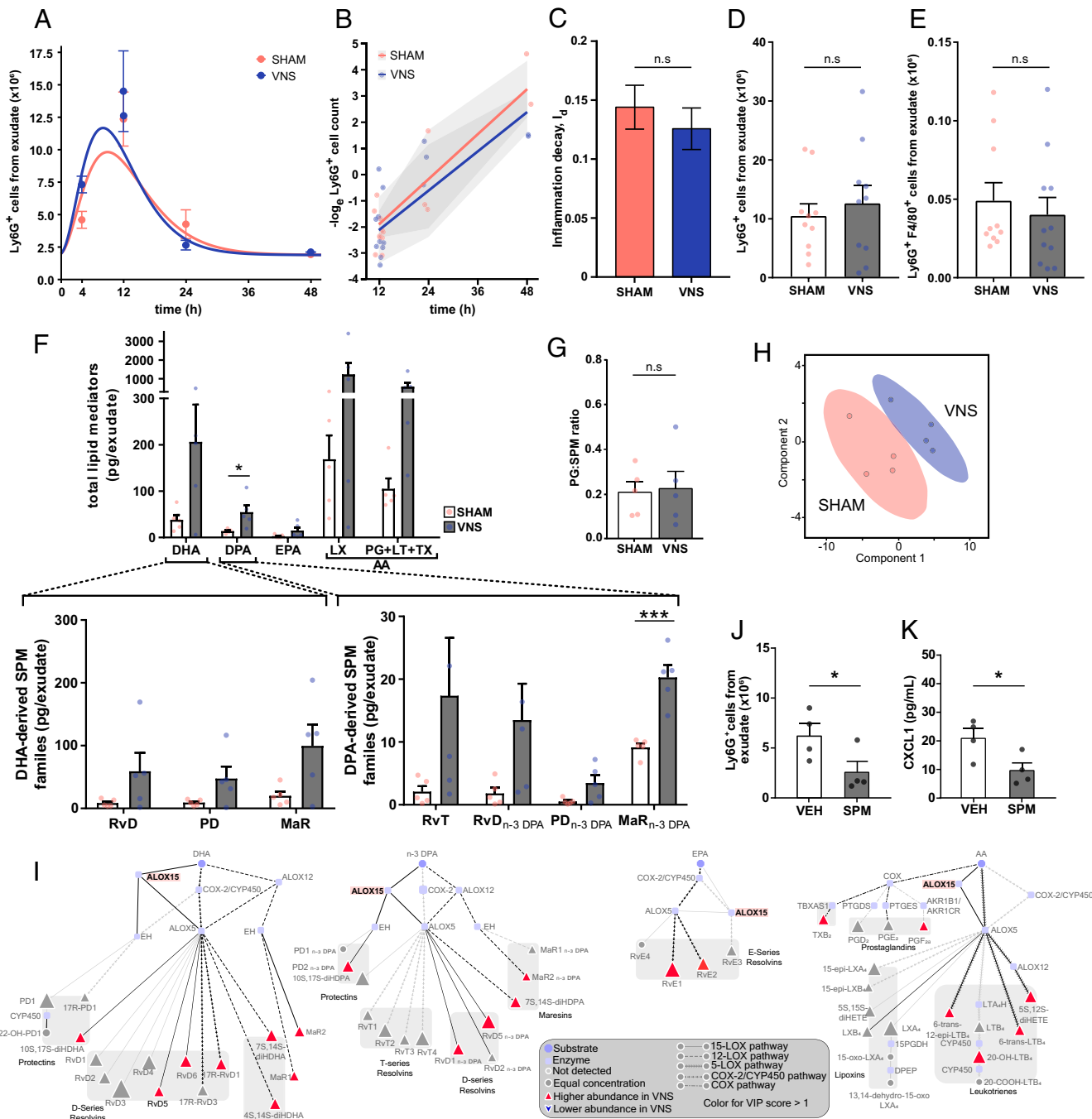
Fig. 4. The α7nAChR was essential for vagus nerve–mediated regulation of inflammation decay (I_d). α7nAChR-deficient mice were subjected to either left cervical VNS or sham surgery followed by intraperitoneal injection of zymosan. Peritoneal exudates were collected at indicated time points after zymosan challenge and analyzed by flow cytometry. (A) Number of Ly6G^{+} cells plotted over time (dots) and modeled using an ODE model (lines). (B) The $\log_e$ cell counts (dots) plotted over time and linear regression analysis (lines), with shaded areas indicating the mean squared error. (C) Rate of inflammation resolution expressed as the inflammation decay (I_d) in sham- (red) and VNS-treated (blue) mice. Results in A–C are from $n = 3$ experiments. (D) Peritoneal exudate Ly6G^{+} cell counts in sham- (red) and VNS-treated (blue) mice at 12 h after zymosan-induced peritonitis. (E) Efferocytosis plotted as absolute numbers of F4/80[+]Ly6G^{+} cells measured by flow cytometry following fixation and intracellular Ly6G staining. Results in D and E are from $n = 3$ experiments. (F) Levels of total LMs identified from the major bioactive metabolomes DHA, DPA, EPA, and AA (LX and PG + LT + TX). Levels of identified DHA-derived SPM families (Lower Left) and n-3 DPA–derived SPM families (Lower Right) in peritoneal exudates from VNS- (blue dots and gray bars) and sham-treated (red dots and open bars) α7nAChR-deficient mice. (G) Ratios of proinflammatory PGs to SPM in peritoneal exudates from VNS- (blue dots and gray bar) and sham-treated (red dots and open bar) α7nAChR-deficient mice. Concentrations of identified and quantified LMs were evaluated using PLS-DA, generating (H) a two-dimensional score plot of LMs in peritoneal exudates from VNS- (blue) and sham-treated (red) mice. (I) LM profiles in VNS- and sham-treated α7nAChR-deficient mice were investigated using an interaction network pathway analysis. (J) α7nAChR-deficient mice were injected with an SPM mixture containing MaR2, RvD2, RvD5, 17R-RvD3 (50 ng of each compound), or vehicle (1.25% EtOH [vol/vol]) immediately prior to induction of zymosan peritonitis, and peritoneal exudates were collected at 12 h. Peritoneal exudate Ly6G^{+} cell counts and (K) CXCL1 levels in supernatants of peritoneal exudates were measured by flow cytometry or MSD multiplex assay in SPM- (gray bar) and vehicle-treated (open bar) mice. Results in F–H and K are from $n = 2$ experiments. Results in C–F are shown as mean ± SEM. n.s. = not significant; *$P < 0.05$; ***$P < 0.001$.

peritonitis, SPM-treated mice had significantly lower numbers of Ly6G$^+$ neutrophils and a significantly lower concentration of CXCL1 in peritoneal exudates as compared with vehicle-treated mice (Fig. 4 *J* and *K*). Taken together, these results demonstrate that the α7nAChR plays an important role in neural regulation of inflammation decay, but deficiency in the receptor can be overcome by injection of synthetic SPM.

Discussion

In this study, we found that VNS accelerated resolution of inflammation. Activation of the vagus nerve promoted efferocytosis and shifted the LM balance toward a more proresolving profile in wild-type mice with peritonitis. VNS-mediated acceleration of resolution was impaired in mice genetically deficient in either Alox15, a key enzyme in LM biosynthesis, or the ACh receptor subunit α7nAChR, which is commonly found on immune cells. Together, these observations demonstrate that the vagus nerve controls resolution of inflammation by cholinergic regulation of the inflammation microenvironment and SPM biosynthesis.

Inflammation resolution is characterized by cessation of neutrophil infiltration and increased efferocytosis (36). Studies pioneered by the laboratory of Serhan and coworkers (22, 29) showed that mice that were vagotomized 7 d before initiation of peritonitis had higher peak neutrophil numbers and delayed resolution of inflammation compared with vagus nerve–intact mice, supporting a role for the vagus nerve in the regulation of peritoneal inflammation. In the present study, we observed that activation of the vagus nerve by electrical stimulation shortened resolution time compared with in sham-treated mice in zymosan-induced peritonitis. Importantly, this study shows that activation of the vagus nerve accelerated the resolution phase of inflammation and exerted cholinergic control of SPM biosynthesis and efferocytosis.

VNS enhanced the production of specific DHA- and n-3 DPA–derived SPMs in peritoneal exudates during inflammation resolution in vivo. In particular, VNS enhanced biosynthesis of the RvD, PD, and MaR families, as demonstrated through identification of RvD2,17R-PD1, and MaR2 as well as their pathway markers 10S,17S-diHDHA (PDX) and 7S,14S-diHDHA, respectively, that are biosynthesized via double lipoxygenation (37). While many mechanistic details of SPM biology, such as their precise mode of action in different inflammatory contexts and the cognate receptors for some of the compounds, at present are incompletely defined, the activity of several compounds (for example, MaR1, RvD2, RvD3, RvD5, RvE1, PD1, and LxA$_4$) was evidenced by the effect on resolution when administered in experimental inflammatory conditions (28, 30, 31, 38). The VNS-dependent regulation of Alox15-dependent LMs reported here indicates that activation of signals in the vagus nerve can shift the balance of LMs during inflammation toward a more proresolving state. This notion is evidenced by the up-regulation of MaR2, RvD2, 17R-PD1, and 10S,17S-diHDHA in the vagus nerve–stimulated mice. As part of their key characteristics, SPMs, including MaR2, RvD2, and PD1, are potent regulators of macrophage phagocytosis and neutrophil trafficking to sites of inflammation (39–41). PD1, also termed neuroprotection D1, is neuroprotective (37, 40), and MaR1, in addition to its potent proresolving actions with immune cells, is also neuroprotective and enhances recovery from spinal cord injury (42). Furthermore, RvD2 and 17R-RvD3, which accelerate resolution of inflammation (42), were also associated with the separation of the VNS and sham clusters on the PLS-DA plot (Fig. 2*A*). These observations also

infer that VNS accelerates inflammation resolution and enhances efferocytosis by activating the Alox15 biosynthetic pathways, a key enzyme in SPM biosynthesis (37). Of note, cyclooxygenase-derived PG and TX were not significantly altered by VNS in wild-type mice, indicating that the vagus nerve may specifically regulate lipoxygenase but not cyclooxygenase biosynthetic pathways, which resulted in an overall proresolving LM profile in exudates from wild-type mice. An imbalance in SPM to proinflammatory eicosanoids (PG, TX, and LT) has been connected with chronic disease progression, including impaired efferocytosis associated with advanced atherosclerotic lesions (2). Additionally, the ratio of SPM to proinflammatory LT or PG is being proposed as a potential biomarker or measure of nonresolving cardiovascular inflammation (43–45). Taken together, these results show that VNS can increase SPM production and accelerate resolution of inflammation in vivo, providing a potential means to activate resolution in chronic inflammatory conditions.

VNS is known to regulate the release of proinflammatory cytokines in early stages of inflammation through an α7nAChR-dependent mechanism (9, 11, 13, 14), and activation of α7nAChR attenuates inflammation in experimental models of chronic disease (46–48). In the present study, the α7nAChR was also required for the VNS-mediated effect on resolution of inflammation in peritonitis (Fig. 4) (13, 15). As expected from studies of acute inflammation, levels of IL-1β and IL-6 were decreased in exudates of VNS-treated wild-type mice compared with sham 12 h after zymosan-induced peritonitis. We did not observe any significant effect by VNS treatment on TNF levels at 12 h after zymosan administration, likely because TNF levels are known to peak early in this model and are considerably reduced toward baseline at 12 h (49, 50). Furthermore, there were no significant differences in the levels of measured cytokines 24 h after zymosan injection. The lack of significant difference between VNS- and sham-treated wild-type mice on levels of the neutrophil chemoattractant, CXCL1, suggests that neutrophil egress and efferocytosis play a role in the reduction of resolution time (R_i) and the increase in inflammation decay (I_d) by VNS. These observations together support the notion that SPMs that rely on biosynthesis by Alox15 are important mediators of resolution of inflammation regulated by cholinergic signals elicited by the vagus nerve in this model.

ACh is a key neurotransmitter in the inflammatory reflex, and VNS increases ACh in the spleen (7, 13, 14). ACh also up-regulates the Alox15 biosynthetic pathway in both human and mouse cells (29). Congruently, ACh up-regulates the RvD and PD biosynthetic pathway marker 17-HDHA in innate lymphoid cells group 3 (29). Interestingly, the peritoneum in rodents is innervated by the vagus nerve (51), and peritoneal ACh levels are reduced in peritonitis after vagotomy (22). It is possible that peritoneal ACh levels regulated by the vagus nerve control resolution of peritoneal inflammation through activation of α7nAChR on innate immune cells (11, 13, 15). Our findings here (that the VNS treatment on α7nAChR-deficient mice failed to reduce neutrophil numbers and levels of proinflammatory cytokines during the resolution phase of zymosan-induced peritonitis) further support that cholinergic signaling is important for the effective resolution of inflammation and depends, at least partly, on the α7nAChR. Of note, injection of a set of synthetic SPMs into α7nAChR-deficient mice reduced neutrophil numbers in peritoneal exudates after zymosan injection, demonstrating that while the α7nAChR is essential for neural regulation of SPM biosynthesis, it is not required for the effect of SPMs.

The use of mathematical modeling of the dynamic changes in local neutrophil numbers here facilitated analysis of the inflammation resolution phase. Our analysis of data from previous studies of neutrophil counts over the course of an episode of peritonitis revealed that the change in neutrophil counts over time showed exponential decay (*SI Appendix*, Fig. S3). In addition to conventional determination of resolution indices (*SI Appendix*, Fig. S2B), the model of exponential decay permits calculation of key indices of inflammation resolution without precise knowledge of the peak time or peak numbers of neutrophil infiltration, points that are challenging to experimentally determine and compare. Accordingly, we add to the indices of resolution the rate of "inflammation decay," I_d, as a measure of the speed with which inflammation resolves.

Three genetically different mouse models were used in this study. A limitation is that the genetic modifications in question have important effects on the immune system. Alox15-deficient mice are known to show lower intensity of the immune response, particularly neutrophil infiltration (52, 53), precluding direct comparisons of the absolute values of neutrophil numbers with the other two models. The α7nAChR-deficient mice have impaired regulation of inflammation with significantly increased cytokine release in proinflammatory events (13), and in the long-term, α7nAChR deficiency may increase the propensity to develop inflammatory diseases. For example, ablation of α7nAChR in hematopoietic cells promotes vascular inflammation and atherosclerosis (54). Therefore, it must be considered that the baseline status of the immune systems in the three models is dissimilar and that direct comparisons between the genotypes are challenging.

While there was no significant difference in the inflammation decay between VNS- and sham-treated Alox15-deficient mice, we did note a difference in the mean numbers of peritoneal exudate neutrophils, with lower numbers and higher mean I_d in the VNS-treated group than in the sham, but the observations were not statistically significant. Of note, VNS treatment did have a significant effect on levels of several non–Alox15-dependent LMs in both Alox15-deficient and α7nAChR-deficient mice, although the relative effect on LMs was opposite between the strains, the mechanism of which is yet not known. It is conceivable that the effects by VNS on resolution of inflammation are not restricted to regulation of Alox15-dependent mediators. In support of this notion, the relative differences in the mean numbers of peritoneal exudate neutrophils were much smaller between VNS- and sham-treated animals in

the α7nAChR-deficient mice, and there was less separation between VNS- and sham-treated animals by PLS-DA in α7nAChR-deficient mice compared with both Alox15-deficient and wild-type mice. The observations in the three different mouse strains together suggest that the α7nAChR is essential for VNS-mediated regulation of the inflammation decay in this model, and while likely not alone responsible for the entire effect, Alox15 is a component of this regulation.

Together, these observations demonstrate that VNS promotes resolution of inflammation in vivo through a mechanism that involves SPM biosynthesis and requires cholinergic signaling. The findings encourage further exploration of neural regulation in resolution of inflammation.

Conclusion

Electrical VNS enhanced biosynthesis of SPMs, increased efferocytosis, and reduced resolution of inflammation in zymosan-induced peritonitis in vivo through a mechanism that involved Alox15 and required the α7nAChR.

Author affiliations: [a]Laboratory of Immunobiology, Division of Cardiovascular Medicine, Department of Medicine, Solna, Karolinska Institutet, Stockholm, 171 76, Sweden; [b]Stockholm Center for Bioelectronic Medicine, MedTechLabs, Karolinska University Hospital, Solna, 171 76, Sweden; [c]William Harvey Research Institute, Barts and The London School of Medicine and Dentistry, Queen Mary University of London, London, EC1M 6BQ, United Kingdom; [d]Department of Mathematics, KTH Royal Institute of Technology, Stockholm, 114 28, Sweden; and [e]Institute of Bioelectronic Medicine, Feinstein Institutes for Medical Research, Manhasset, New York, 11030

Author contributions: A.S.C., H.A., and P.S.O. designed research; A.S.C., A.L.G., L.T., R.A.C., J.D., and H.A. performed research; J.D., H.H., and H.A. contributed new reagents/analytic tools; A.S.C., A.L.G., L.T., V.S.S., R.A.C., J.D., H.H., H.A., and P.S.O. analyzed data; A.L.G., L.T., and S.G.M. discussed data and revised the paper throughout the project; and A.S.C., H.A., and P.S.O. wrote the paper.

1. C. N. Serhan, Pro-resolving lipid mediators are leads for resolution physiology. *Nature* **510**, 92–101 (2014).
2. G. Fredman *et al.*, An imbalance between specialized pro-resolving lipid mediators and pro-inflammatory leukotrienes promotes instability of atherosclerotic plaques. *Nat. Commun.* **7**, 12859 (2016).
3. C. N. Serhan, N. Chiang, J. Dalli, The resolution code of acute inflammation: Novel pro-resolving lipid mediators in resolution. *Semin. Immunol.* **27**, 200–215 (2015).
4. G. Schett, M. F. Neurath, Resolution of chronic inflammatory disease: Universal and tissue-specific concepts. *Nat. Commun.* **9**, 3261 (2018).
5. M. A. Sugimoto, L. P. Sousa, V. Pinho, M. Perretti, M. M. Teixeira, Resolution of inflammation: What controls its onset? *Front. Immunol.* **7**, 160 (2016).
6. J. N. Fullerton, D. W. Gilroy, Resolution of inflammation: A new therapeutic frontier. *Nat. Rev. Drug Discov.* **15**, 551–567 (2016).
7. P. S. Olofsson, M. Rosas-Ballina, Y. A. Levine, K. J. Tracey, Rethinking inflammation: Neural circuits in the regulation of immunity. *Immunol. Rev.* **248**, 188–204 (2012).
8. V. A. Pavlov, S. S. Chavan, K. J. Tracey, Molecular and functional neuroscience in immunity. *Annu. Rev. Immunol.* **36**, 783–812 (2018).
9. L. V. Borovikova *et al.*, Vagus nerve stimulation attenuates the systemic inflammatory response to endotoxin. *Nature* **405**, 458–462 (2000).
10. P. S. Olofsson *et al.*, Single-pulse and unidirectional electrical activation of the cervical vagus nerve reduces TNF in endotoxemia. *Bioelectron. Med.* **2**, 37–42 (2015).
11. L. Tarnawski *et al.*, Adenylyl cyclase 6 mediates inhibition of TNF in the inflammatory reflex. *Front. Immunol.* **9**, 2648 (2018).
12. A. S. Caravaca *et al.*, An effective method for acute vagus nerve stimulation in experimental inflammation. *Front. Neurosci.* **13**, 877 (2019).
13. H. Wang *et al.*, Nicotinic acetylcholine receptor α7 subunit is an essential regulator of inflammation. *Nature* **421**, 384–388 (2003).
14. M. Rosas-Ballina, P. S. Olofsson, M. Ochani, S. I. Valdes-Ferrer, Y. A. Levine, C. Reardon *et al.*, Acetylcholine-synthesizing T cells relay neural signals in a vagus nerve circuit. *Science* **334**, 98–101 (2011).
15. P. S. Olofsson *et al.*, α7 nicotinic acetylcholine receptor (α7nAChR) expression in bone marrow-derived non-T cells is required for the inflammatory reflex. *Mol. Med.* **18**, 539–543 (2012).
16. F. A. Koopman *et al.*, Vagus nerve stimulation inhibits cytokine production and attenuates disease severity in rheumatoid arthritis. *Proc. Natl. Acad. Sci. U.S.A.* **113**, 8284–8289 (2016).
17. M. Eberhardson, L. Tarnawski, M. Centa, P. S. Olofsson, Neural control of inflammation: Bioelectronic medicine in treatment of chronic inflammatory disease. *Cold Spring Harb. Perspect. Med.* **10**, a034181 (2020).
18. D. van Westerloo, T. van der Poll, Acute vagotomy activates the cholinergic anti-inflammatory pathway. *Am. J. Physiol. Heart Circ. Physiol.* **288**, H977–H978 (2005).
19. D. J. van Westerloo *et al.*, The cholinergic anti-inflammatory pathway regulates the host response during septic peritonitis. *J. Infect. Dis.* **191**, 2138–2148 (2005).
20. D. J. van Westerloo *et al.*, The vagus nerve and nicotinic receptors modulate experimental pancreatitis severity in mice. *Gastroenterology* **130**, 1822–1830 (2006).
21. V. A. Pavlov, K. J. Tracey, Neural regulation of immunity: Molecular mechanisms and clinical translation. *Nat. Neurosci.* **20**, 156–166 (2017).
22. V. Mirakaj, J. Dalli, T. Granja, P. Rosenberger, C. N. Serhan, Vagus nerve controls resolution and pro-resolving mediators of inflammation. *J. Exp. Med.* **211**, 1037–1048 (2014).
23. C. N. Serhan, X. de la Rosa, C. C. Jouvene, X. de la Rosa, C. C. Jouvene, Cutting edge: Human vagus produces specialized proresolving mediators of inflammation with electrical stimulation reducing proinflammatory eicosanoids. *J. Immunol.* **201**, 3161–3165 (2018).

24. R. A. Colas, E. A. Gomez, J. Dalli, Methodologies and procedures employed in the identification and quantitation of lipid mediators via LC-MS/MS. ResearchGate [Preprint] (2020). https://www.researchgate.net/publication/346484981_Methodologies_and_Procedures_Employed_in_the_Identification_and_Quantitation_of_Lipid_Mediators_via_LC-MSMS (Accessed 13 January 2022).

25. E. A. Gomez et al., Blood pro-resolving mediators are linked with synovial pathology and are predictive of DMARD responsiveness in rheumatoid arthritis. Nat. Commun. 11, 5420 (2020).

26. P. R. Souza et al., The GPR40 agonist GW9508 enhances neutrophil function to aid bacterial clearance during E. coli infections. Front. Immunol. 11, 573019 (2020).

27. V. B. Odonnell et al., Steps toward minimal reporting standards for lipidomics mass spectrometry in biomedical research publications. Circ. Genom. Precis. Med. 13, 737–741 (2020).

28. G. L. Bannenberg et al., Molecular circuits of resolution: Formation and actions of resolvins and protectins. J. Immunol. 174, 4345–4355 (2005).

29. J. Dalli, R. A. Colas, H. Arnardottir, C. N. Serhan, Vagal regulation of Group 3 innate lymphoid cells and the immunoresolvent PCTR1 controls infection resolution. Immunity 46, 92–105 (2017).

30. H. Arnardottir, S. K. Orr, J. Dalli, C. N. Serhan, Human milk proresolving mediators stimulate resolution of acute inflammation. Mucosal Immunol. 9, 757–766 (2016).

31. H. H. Arnardottir, J. Dalli, R. A. Colas, M. Shinohara, C. N. Serhan, Aging delays resolution of acute inflammation in mice: Reprogramming the host response with novel nano-proresolving medicines. J. Immunol. 193, 4235–4244 (2014).

32. C. Godson et al., Cutting edge: Lipoxins rapidly stimulate nonphlogistic phagocytosis of apoptotic neutrophils by monocyte-derived macrophages. J. Immunol. 164, 1663–1667 (2000).

33. J. Dalli, R. A. Colas, M. E. Walker, C. N. Serhan, Lipid mediator metabolomics via LC-MS/MS profiling and analysis. Methods Mol. Biol. 1730, 59–72 (2018).

34. K. A. Janes, M. B. Yaffe, Data-driven modelling of signal-transduction networks. Nat. Rev. Mol. Cell Biol. 7, 820–828 (2006).

35. I. G. Chong, C. H. Jun, Performance of some variable selection methods when multicollinearity is present. Chemom. Intell. Lab. Syst. 78, 103–112 (2005).

36. C. N. Serhan, N. Chiang, B. D. Levy, Lipid mediators in the resolution of inflammation. Cold Spring Harb. Perspect. Biol. 7, a016311 (2014).

37. C. N. Serhan, J. Dalli, R. A. Colas, J. W. Winkler, N. Chiang, Protectins and maresins: New pro-resolving families of mediators in acute inflammation and resolution bioactive metabolome. Biochim. Biophys. Acta 1851, 397–413 (2015).

38. N. Chiang et al., Infection regulates pro-resolving mediators that lower antibiotic requirements. Nature 484, 524–528 (2012).

39. J. M. Schwab, N. Chiang, M. Arita, C. N. Serhan, Resolvin E1 and protectin D1 activate inflammation-resolution programmes. Nature 447, 869–874 (2007).

40. B. Deng et al., Maresin biosynthesis and identification of Maresin 2, a new anti-inflammatory and pro-resolving mediator from human macrophages. PLoS One. 9, e102362 (2014).

41. N. Chiang, J. Dalli, R. A. Colas, C. N. Serhan, Identification of resolvin D2 receptor mediating resolution of infections and organ protection. J. Exp. Med. 212, 1203–1217 (2015).

42. I. Francos-Quijorna et al., Maresin 1 promotes inflammatory resolution, neuroprotection, and functional neurological recovery after spinal cord injury. J. Neurosci. 37, 11731–11743 (2017).

43. S. Thul, C. Labat, M. Temmar, A. Benetos, M. Bäck, Low salivary resolvin D1 to leukotriene B$_4$ ratio predicts carotid intima media thickness: A novel biomarker of non-resolving vascular inflammation. Eur. J. Prev. Cardiol. 24, 903–906 (2017).

44. H. A. Bazan et al., Circulating inflammation-resolving lipid mediators RvD1 and DHA are decreased in patients with acutely symptomatic carotid disease. Prostaglandins Leukot. Essent. Fatty Acids 125, 43–47 (2017).

45. M. Carracedo, G. Artiach, H. Arnardottir, M. Bäck, The resolution of inflammation through omega-3 fatty acids in atherosclerosis, intimal hyperplasia, and vascular calcification. Semin. Immunopathol. 41, 757–766 (2019).

46. A. Bruchfeld et al., Whole blood cytokine attenuation by cholinergic agonists ex vivo and relationship to vagus nerve activity in rheumatoid arthritis. J. Intern. Med. 268, 94–101 (2010).

47. T. Hashimoto et al., Stimulation of α7 nicotinic acetylcholine receptor by AR-R17779 suppresses atherosclerosis and aortic aneurysm formation in apolipoprotein E-deficient mice. Vascul. Pharmacol. 61, 49–55 (2014).

48. L. Galle-Treger et al., Nicotinic acetylcholine receptor agonist attenuates ILC2-dependent airway hyperreactivity. Nat. Commun. 7, 13202 (2016).

49. Z. Bian, Y. Guo, B. Ha, K. Zen, Y. Liu, Regulation of the inflammatory response: Enhancing neutrophil infiltration under chronic inflammatory conditions. J. Immunol. 188, 844–853 (2012).

50. Y. Zhang, B. F. Ramos, B. A. Jakschik. Neutrophil recruitment by tumor necrosis factor from mast cells in immune complex peritonitis. Science 258, 1957–1959 (1992).

51. K. Tanaka, T. Matsugami, T. Chiba, The origin of sensory innervation of the peritoneum in the rat. Anat. Embryol. (Berl.) 205, 307–313 (2002).

52. K. Gronert et al., A role for the mouse 12/15-lipoxygenase pathway in promoting epithelial wound healing and host defense. J. Biol. Chem. 280, 15267–15278 (2005).

53. J. Rossaint, J. L. Nadler, K. Ley, A. Zarbock, Eliminating or blocking 12/15-lipoxygenase reduces neutrophil recruitment in mouse models of acute lung injury. Crit. Care 16, R166 (2012).

54. M. E. Johansson et al., α7 Nicotinic acetylcholine receptor is expressed in human atherosclerosis and inhibits disease in mice–Brief report. Arterioscler. Thromb. Vasc. Biol. 34, 2632–2636 (2014).